IMPROVED SURFACE WAVE DETECTION AND MEASUREMENT USING PHASE-MATCHED FILTERING AND IMPROVED REGIONALIZED MODELS

Jeffry L. Stevens and David A. Adams
Maxwell Technologies, Systems Division

Sponsored by U. S. Department of Defense
Defense Threat Reduction Agency

Contract No. DSWA01-98-C-0154

ABSTRACT

The goal of this project is to improve the capability to identify and detect surface waves under a Comprehensive Nuclear-Test-Ban Treaty. To date, we have concentrated on two tasks: development of improved regionalized earth models and dispersion curves, and improvements to surface wave processing through implementation of phase-matched filtering and path corrected spectral magnitudes. The first objective is to improve the dispersion curves that are now in use at the International Data Centre (IDC). The global dispersion data set has been expanded and now contains over 248,000 data points. Two global tomographic inversions were performed using this data set. The first inversion used the 149 IDC models as starting models. With the expanded data set regions such as Antarctica and Saudi Arabia where coverage was better were significantly improved. The second inversion increased the number of models to 399 to provide additional degrees of freedom in regions that required them. This inversion significantly improved the data fit in Eurasia and the Middle East. The standard deviation in the error of dispersion curves along paths from the former East Kazakh nuclear test site was reduced by almost a factor of two. We are continuing to make improvements to the models by adding new data, applying constraints where available, and adding models where the data requires them.

Automatic identification of surface waves at the International Data Center is currently performed by narrow-band filtering the data at several frequencies, and then comparing the arrival times with a regionalized dispersion model. We would like to improve the performance of the surface wave detector using phase-matched filtering and are in the process of identifying the optimum procedure for doing so. Some obvious ways of using the phase-matched filtered waveform, such as using an STA/LTA identification technique, do not work as well as the current narrow-band filtering procedure. Narrow band filtering has the advantage of being a very stable method of determining frequency-dependent arrival times. Consequently, we have tried a new approach in which we apply narrow-band filters to the compressed waveform and use a detection test similar to the current test. This allows us to take advantage of the improved signal to noise ratio of the phase-match filtered waveforms, while retaining the robustness of narrow-band filtering for frequency dependent signal identification. After phase-matched filtering, the predicted arrival time is zero at all frequencies, so we test to see if the arrivals are within a time window similar to that used in the existing test. To test the performance of this technique, we added the capability of performing this analysis to Maxpmf, which is a version of the automatic processing code Maxsurf with phase-matched filtering added. We then processed two days of data from the data archive at the PIDC and compared the results with the reviewed event bulletin. The number of detections increased by about 15%. This is a good indication that the method is a significant improvement over current techniques, and we are working on optimizing the technique to obtain further improvements.

Objective

The goal of this project is to improve the capability to identify and detect surface waves under a CTBT in order to improve event screening using the M_s:m_b discriminant. This is being accomplished through development of improved regionalized phase and group velocity models, development of regionalized path corrected spectral magnitudes, and improvement of automated surface wave detection using phase-matched filtering.

Research Accomplished

During the first half of this project we have concentrated primarily on two tasks:

1. Improvement of regionalized global earth models and dispersion curves.
2. Automatic surface wave identification using phase-matched filtering.

There are several tasks to be performed under this contract, and we have focused on these first because 1) all of the tasks require a global earth model and dispersion curves, and optimizing these will improve all other results; and 2) the most immediate practical result of this work will be the improvement of automatic processing of surface waves, and automatic processing of surface waves in turn provides a test of the dispersion curves. In this paper, we first discuss the techniques we have been using to improve the earth models and dispersion curves, and then discuss an improvement to the current surface wave identification procedures using phase-matched filtering.

Development of Regionalized Earth Models

We are developing improved models of earth structure in order to predict surface wave behavior more accurately. These models are important for calculating path corrections for spectral magnitudes, for constructing phase matched filters, and for better prediction of group velocity arrival times used in existence tests in automatic surface wave processing.

Our global models currently consist of 2592 5x5 degree cells, each one associated with a particular model type. There are far fewer model types than cells. Each model type consists of plane layers, each with uniform P and S wave velocities, density and Q, with layers extending to a depth of about 200 km. We treat the S-wave velocities as free parameters which are estimated by tomographic inversion of observations of group and phase velocity dispersion of surface waves. The surface wave dispersion observations come from a variety of surface wave studies and from GSETT3 PIDC data.

Stevens and McLaughlin (2000) describe development of a global earth model with 149 distinct models on a five degree grid that is now used for surface wave identification at the PIDC and IDC. The development used global tomographic inversion of about 90,000 dispersion measurements, using the Crust 5.1 model (Mooney, et al., 1998) as a starting point. This process was continued by Stevens and Adams (1999) who increased the number of data points to more than 164,000 and increased the number of earth model types to 230. We have carried the process still further by increasing the number of model types to 399 and the number of data points to more than 248,000. The total number of free parameters in this case is 5147.

The number of free parameters in the global model can be increased as the number of data points is increased. We describe below procedures for finding new model types. Estimates of S-wave velocities are sensitive to the slower sedimentary layers, especially for higher frequencies. We describe corrections for this effect. Inversions have been performed both with P-wave velocities fixed (by Crust 5.1 or other studies), and with the P-wave velocities constrained by Poisson's ratio, and densities by Birch's Law.

Finding new model types

Addition of new data permits us to increase the number of model types and therefore the total number of free parameters. To select new model types we have been using the results of 2D group velocity tomography to identify cells with the largest perturbations in velocity (Stevens and Adams, 1999). "2D tomography" refers to the more traditional type of tomographic inversion in which we invert observed group velocity dispersion measurements over a narrow frequency band to find the group velocities for each cell on the 5 degree grid. Thus for each of 9 frequency bands we preform a tomographic inversion using the group velocity residuals from the 3D tomographic inversion (inversion for earth structure using both phase and group velocity at all frequencies) as data, and perturbations in the group velocities for each of the 2592 cells as parameters. Cells with large perturbations for several frequency bands are selected as possible candidates for association with new model types. The underlying reason is that cells with the large perturbations are the ones most

constrained, in the 3D inversion, by belonging to a particular type. One problem with this approach is that spurious large perturbations can occur in areas of poor resolution. Therefore, as an additional guide, we now compute resolution matrices of the 2D tomographic systems of equations. Thus well resolved cells with large group velocity perturbations are given new model types and poorly resolved cells with large perturbations are not unless there is other supporting evidence. We are using the Lanczos method of approximating SVDs for sparse matrices described and applied to tomography problems by Vasco *et al.* (1999), and code written by Berry (1992).

Figure 1 shows the diagonal elements of an approximation of the resolution matrix for the 2D tomographic system using group velocity measurements for frequencies above and including 0.025 Hz and below 0.0330 Hz. This approximation is made by computing only the 573 most significant singular values of the SVD out of a possible 2592 (the number of cells) and using the 573 corresponding singular vectors to approximate R, i.e. $R=V_pV_p^T$. V_p is the rectangular 2952x573 submatrix of V where V is defined by the Lanczos decomposition of the full matrix $A=USV^T$.

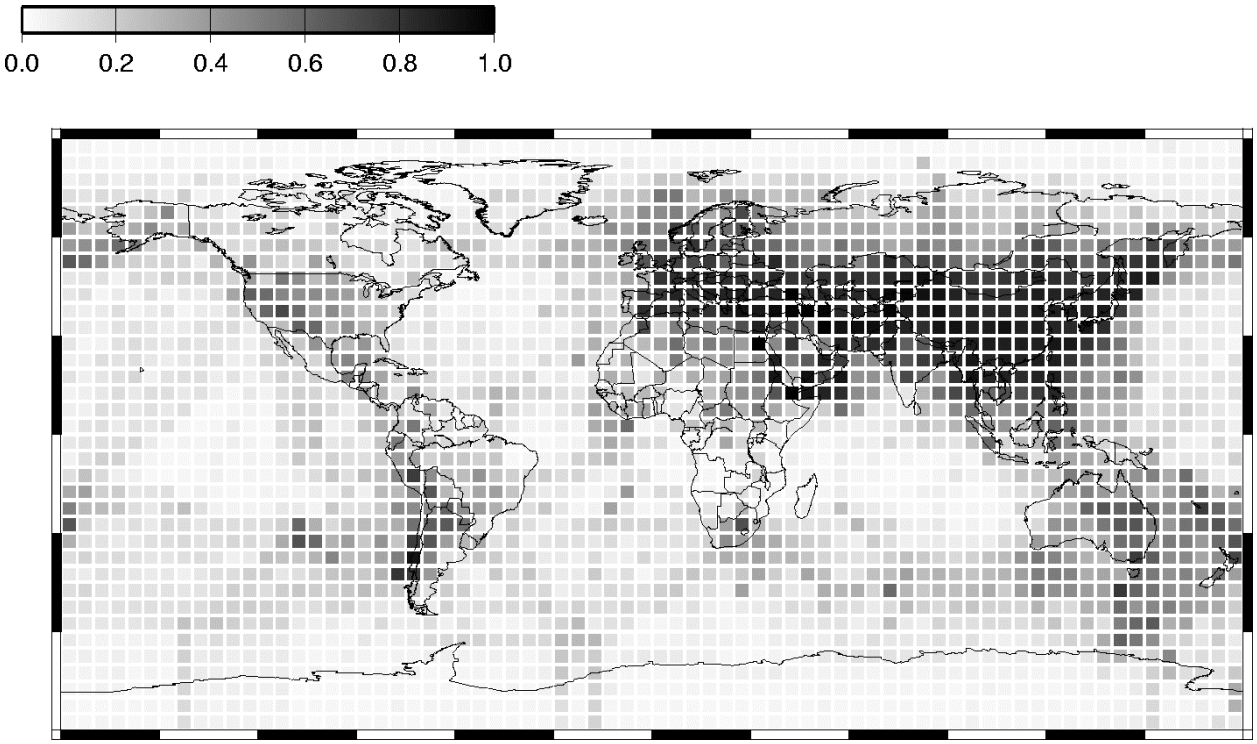

Figure 1. Map of the diagonal elements of the resolution matrix for group velocity measurements in the frequency range 0.025 to .0330 Hz using an approximation of the SVD using the Lanczos method and 573 out of a possible 2592 singular values.

Selection of new model types from resolution calculations

We computed the resolution matrices for the 2D group velocity tomographies for eight frequency bands: below 0.01 Hz, 0.01 to 0.0140 Hz, 0.0140 to 0.0167 Hz, 0.0167 to 0.025 Hz, 0.025 to 0.033 Hz, 0.033 to 0.04 Hz, 0.04 to 0.05 Hz, 0.05 to 0.067 Hz. Those cells associated with diagonal components of resolution matrices greater than 0.6 for 8 frequencies were given new model types. The 0.6 value for a cell means that there is some smearing among other cells but that the true perturbation of the cell contributes the most (60%) to the tomographic value. The new types had the same number of layers and layer thicknesses as the originating types, and the initial parameters were set the same. All of these types are found in Asia and the Middle East.

The addition of these new model types plus those discussed in the following section increases the number of types from 230 to 399 and reduces the weighted standard deviation in data by about 5%.

Selection of new model type for oceanic ridges and the Cocos Plate

Selection of new model types is a fairly complicated process requiring some judgement. Here we give an example of one case that is relatively straightforward because the tomographic results and geophysical constraints provide complementary sets of information. From 2D group velocity tomographies we identified slow regions associated with some oceanic ridges and the Cocos Plate. These observations were used to split a new type A0h from the most populous model type (A0). For each frequency band a 2D group velocity tomography was carried out. The results show an association between slowness perturbation and oceanic ridges which is strongest for the frequency band 0.0167 to 0.025 Hz. This particular slowness perturbation map was chosen to separate A0 type models into two groups of cells with either fast or slow perturbations. The distribution of fast and slow cells is dependent on the slowness value chosen to separate the two groups. In many cases slow type cells were not located at an oceanic ridge. In other cases slow cells were found on a ridge but isolated from other slow cells. Other times a slow group of cells was found at a ridge and was several cells wide. Because the great majority of type A0 cells are not well resolved we relocated some slow cells but never by more than the distance of one cell. For the same reason, we assumed that the ridge types should be in groups only one cell wide, and most single isolated slow cells, especially ones found in plate interiors, were not given the new type. The Cocos Plate now consists of only of cells with the new type. There are many slow types in the interior of the Nazca Plate but we have chosen for now to continue modeling it with the type A0. In the future we may introduce a new Nazca type. Figure 2 shows the locations of cells of the two model types A0 and A0h. After the most recent inversions the A0h velocity structure is slower than the A0 structure between about 10 km and 80 km with a maximum difference of about 1%.

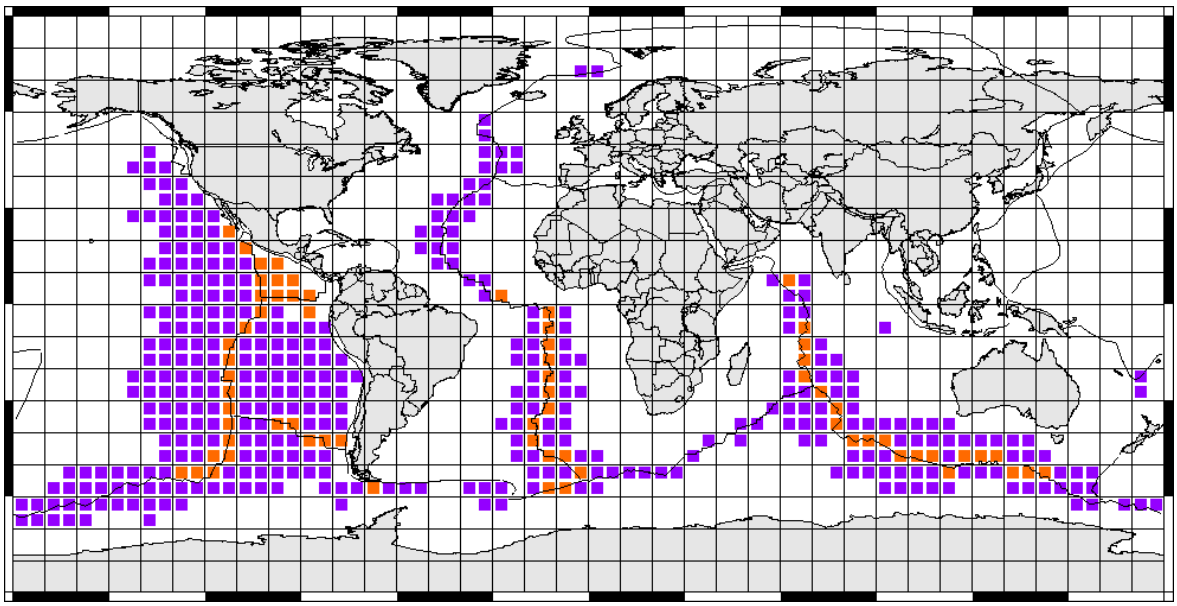

Figure 2. locations of the two model types A0, in purple (or dark gray), and type A0h in orange (or light gray).

Corrections for sedimentary layers and bathymetry

It is important to account for the effects of sediments and, for oceanic model types, the water column. These shallow layers are, in general, too thin to be resolved by the surface wave inversion, yet they do have an effect on the higher frequency parts of the dispersion curves, so these are held fixed when the tomographic inversion is performed. The parameters for the sedimentary layers based on the one degree grid sediment thickness data of Laske and Masters (1997). Their model consists of layer thicknesses, P and S wave velocities and densities

and is still in the process of revision. We use an averaging procedure to incorporate this information into our 5 degree model. Useful information is lost during averaging because the variation of sedimentary parameters within cells can be large. We are in the process of refining this model further, and decreasing the grid spacing to a 1º grid. The surface layers of this model are based on the Laske and Masters sediment maps and high resolution bathymetry maps. The 1º grid will also allow us to define the ocean depths on a finer scale and resolve the ocean/continent boundaries more accurately.

Inversion with fixed Poisson's ratio

The inversions described above used constrained P-wave velocities, fixed to be consistent with the Crust 5.1 models. As the number of models has increased, however, there is increasing inconsistency between the P and S velocities, so the most recent inversions have instead been performed with the P wave velocity and density constrained by the shear velocity. In these inversions, the Poisson's ratio is fixed to 0.25 and the density is governed by Birch's Law. For the inversions with 309 model types the fixed Poisson's ratio models fit the data better with a standard deviation reduction of about 1.5%.

Expanded data set

We have added new dispersion measurements to our data set, the largest consisting of 83,966 phase velocity measurents taken from Curtis et al. (1998) for Eurasia for frequencies between 0.00667 Hz and 0.0385 Hz. This greatly increases the number of phase velocity measurements in the data set. Since group velocities are derived from a derivative of phase velocities, there is a degree of uncertainty in inversion of group velocities that does not exist for phase velocities. Consequently, phase velocities place stronger constraints on the surface wave inversion, and are particularly important at longer periods. Initial inversions of this new data tend to increase the model velocities below about 100 km by a few percent. This brings the total number of data points to be inverted to approximately 248,000. The data set has been derived from a variety of regional and global studies including the following: global surface wave group velocities from earthquakes derived using PIDC GSETT3 data (Stevens and McLaughlin, 1996), augmented with more recent measurements derived from PIDC data; surface wave phase and group velocity dispersion curves from underground nuclear test sites (Stevens, 1986; Stevens and McLaughlin, 1988), calculated from earth models for 270 paths (test site – station combinations) at 10 frequencies between 0.015 and 0.06 Hz; phase and group velocity measurements for western Asia and Saudi Arabia from Mitchell et al.(1996) for 12 paths at 17 frequencies between 0.012 and 0.14 Hz; the global phase velocity model of Ekstrom et al. (1996) for 9 periods between 35 and 150 seconds calculated for each 5 degree grid block from a spherical harmonic expansion of order l=40; group velocity measurements for Eurasia from Ritzwoller et al.(1996) and Levshin et al.(1996) for 20 frequencies between 0.004 and 0.1 Hz with 500 to 5000 paths per frequency; Antarctic and South American group velocity measurements from the University of Colorado (Vdovin et al., 1999; Ritzwoller et al., 1999); and a very large set of dispersion measurements from Saudi Arabia provided by Herrmann and Mokhtar at St. Louis University.

Improvement to data fit

In general, additional data will improve the models primarily in the regions with new data. However, as new data is added, if additional models are not added, the data fit may actually degrade in some regions as the model strains to fit the new data in other regions. One test of the models is to look at the important case of paths from historical nuclear test sites. Tables 1 and 2 show group velocity dispersion residuals and standard deviations in the residuals for periods of 40 seconds and 20 seconds, respectively, for paths from several nuclear test sites. With the expanded data set and 149 models, the results are changed only slightly relative to the inversion with the smaller data set, and in fact the results are degraded slightly for the paths from the test sites. This is because the new data caused larger changes in other areas and with the constraint of the small number of models, the data fit became slightly worse in order to allow larger improvements in the areas with concentrations of new data. With 399 models, however, these constraints are relaxed, and the data fit improves for all test sites, and improves quite dramatically for paths in Asia. In particular the standard deviations of the residuals for paths from the East Kazakh test site are decreased by almost half at 40 seconds and by 25% at 20 seconds.

Table 1. 40 Second Group Velocity % Average Residuals (Standard Deviations)

Source	IDC 5° - 149 Models	#1 - Expanded Data Set	#2 - 399 Models
NTS (59)	0.15 (1.40)	0.22 (1.44)	0.14 (1.20)
East Kazakh (40)	0.80 (2.21)	0.85 (2.45)	0.13 (1.11)
Mururoa (13)	-0.78 (1.43)	-0.73 (1.79)	-0.59 (1.56)
Novaya Zemlya (99)	-0.06 (2.06)	0.01 (2.05)	-0.18 (1.81)
Amchitka (55)	0.25 (1.39)	0.34 (1.39)	0.35 (1.08)

Table 2. 20 Second Group Velocity % Average Residuals (Standard Deviations)

Source	IDC 5°	#1 - Expanded Data Set	#2 - 399 Models
NTS (58)	-0.47 (2.25)	-0.38 (2.23)	-0.30 (1.88)
East Kazakh (40)	-0.75 (1.96)	-0.65 (2.07)	-0.64 (1.44)
Mururoa (11)	0.41 (1.43)	0.41 (1.40)	0.53 (1.36)
Novaya Zemlya (99)	-0.26 (3.61)	-0.23 (3.66)	-0.43 (3.01)
Amchitka (54)	0.83 (3.76)	0.70 (3.74)	0.22 (3.23)

Automatic surface wave processing with phase-matched filtering

Automatic identification of surface waves at the International Data Center is currently performed using the processing program Maxsurf by narrow-band filtering the data at several frequencies and then comparing the arrival times with a regionalized dispersion model. We would like to improve the performance of the surface wave detector by using phase-matched filtering and are in the process of identifying the optimum procedure for doing so. An automatic surface wave processing program, Maxpmf, has been developed which is similar to Maxsurf except that it applies phase-matched filtering to seismograms and calculates path-corrected spectral magnitudes in addition to M_s. Maxpmf integrates a regionalized phase velocity model to generate a phase-matched filter which is used to compress the surface wave waveforms. Figure 3, below, shows an example of waveform compression after application of phase-matched filters to a data set.

Some obvious ways of using the phase-matched filtered waveform, such as using an STA/LTA identification technique, do not work as well as the current narrow-band filtering procedure. Narrow band filtering has the advantage of being a very stable method of determining frequency-dependent arrival times. Consequently, we have tried a new approach in which we apply narrow-band filters to the compressed waveform and use a detection test similar to the current test. This allows us to take advantage of the improved signal to noise ratio of the phase-match filtered waveforms, while retaining the robustness of narrow-band filtering for frequency dependent signal identification. After phase-matched filtering, the predicted arrival time is zero at all frequencies, so we test to see if the arrivals are within a time window similar to that used in the existing test. This is illustrated in Figure 4.

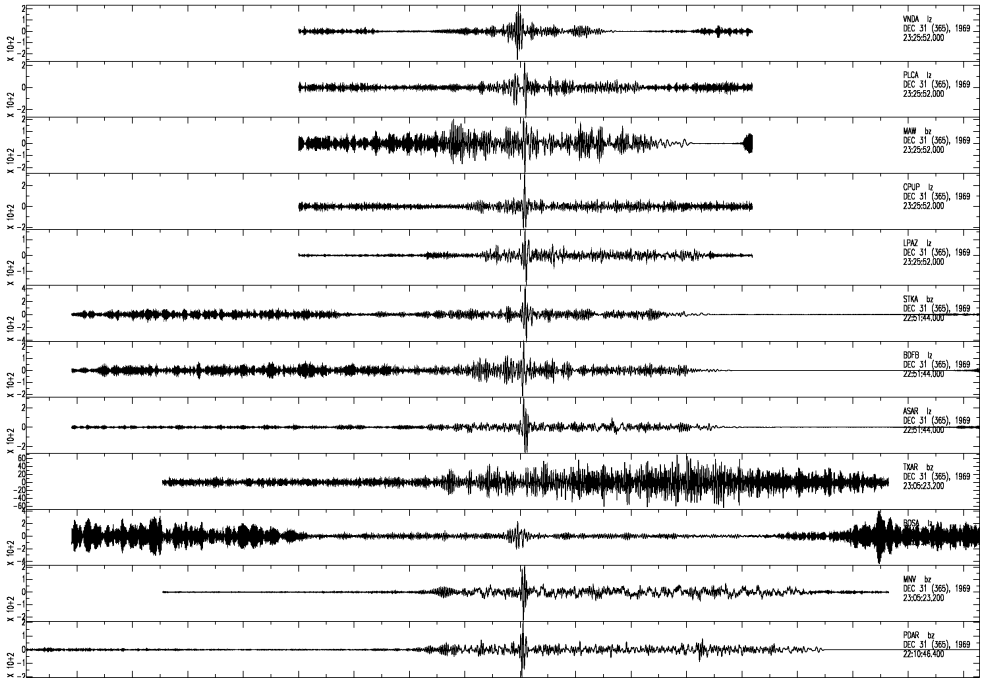

Figure 3. Compressed waveforms after application of phase-matched filters to 12 surface wave seismograms. The data is from an m_b 3.9 South Pacific earthquake that occurred 1997 June 15.

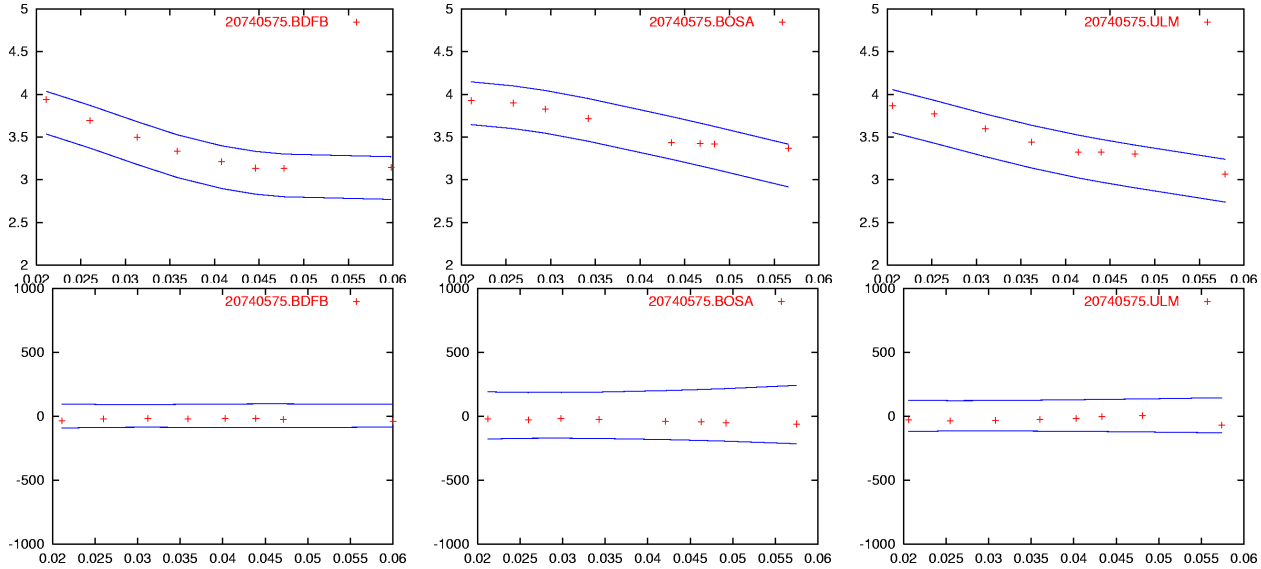

Figure 4. The narrow-band filter detection test (top) compares measured group velocity with a regionalized group velocity model. To improve detection, we phase-match filter the data first, then apply narrow-band filters (bottom). The detection test is applied for the same time interval, but the time is now centered around zero. This example is for an m_b 4.2 South American earthquake observed at BDFB, BOSA, and ULM.

To test the performance of this technique, we added the capability to perform this analysis to Maxpmf, and processed two days of data from the data archive at the PIDC. We then compared the results with the reviewed event bulletin. The number of detections increased by about 15%. This is a good indication that the method is a significant improvement over current techniques, and we are now working on optimizing the technique to obtain further improvements.

CONCLUSIONS AND RECOMMENDATIONS

In this paper, we have described improvements to regionalized dispersion models and phase-matched filtering that are necessary for optimization of surface wave processing under a Comprehensive Nuclear-Test-Ban Treaty. Because the number of events increases rapidly at small magnitudes, a decrease in the threshold of reliable surface wave detection and measurement can greatly reduce the number of unidentified events. Improved surface wave analysis methods can reduce the surface wave magnitude threshold, improve screening capability, and reduce the likelihood of unnecessary on-site inspections under a CTBT. We are continuing to improve the regionalized models and to improve surface wave identification using phase-matched filtering to reduce the threshold for surface wave identification and measurement.

In addition to optimizing procedures for surface wave identification, we are also testing improved procedures for optimizing surface wave measurement. A more stable and reliable measurement of surface wave amplitude than the traditional time domain M_s is the "path corrected spectral magnitude" (Stevens and McLaughlin, 2000; Stevens and Adams, 1999) which corrects the spectral amplitude with a surface wave Green's function and averages over an optimum frequency band. An advantage of the frequency domain processing is that a spectral magnitude of either signal or noise can always be measured over the specified frequency band, while it may not be possible to measure data in a specified frequency band in the time domain. Maxsurf, for example, will reject a seismogram if it can't find a 20 second arrival within the predicted arrival time window. This often occurs at regional distances and there is no reason for such a restriction for spectral magnitudes. Consequently, moments can be measured for regional seismograms in cases where standard M_s measurements cannot be made. During the next year, we will be working to optimize the path corrected spectral magnitude, and will assess the ability of the measurement to improve discrimination.

Acknowledgements

We would like to thank Mike Ritzwoller, Anatoli Levshin and Antonio Villasenor of the University of Colorado, Brian Mitchell and Bob Herrmann of St. Louis University, Goran Ekstrom of Harvard University, Andrew Curtis of Utrecht University, and their coworkers for the use of their data and models in this project**.**

Key Words: surface wave, dispersion curve, phase matched filter, regionalization, moment

REFERENCES

Berry, M. (1992), Large scale singular value computations, *Int. J. Supercomp. Appl., 6, 13-49*.

Curtis, A., J. Trampert, R. Snieder, and B. Dost (1998), Eurasian fundamental mode surface wave phase velocities and their relationship with tectonic structures. *J Geophys. Res., 103 (B11)* 26,919-26,947.

Ekstrom, G., A. M. Dziewonski, G. P. Smith, and W. Su (1996), "Elastic and Inelastic Structure Beneath Eurasia," in *Proceedings of the 18th Annual Seismic Research Symposium on Monitoring a Comprehensive Test Ban Treaty, 4-6 September, 1996*, Phillips Laboratory Report PL-TR-96-2153, July, pp. 309-318, ADA313692.

Herrin, E. and T. Goforth (1977), "Phase-Matched Filtering: Application to the Study of Rayleigh Waves," *Bull. Seism. Soc. Am*., v. 67, pp. 1259-1275.

Laske G., and G. Masters (1997), A Global Digital Map of Sediment Thickness, *EOS Trans. AGU, 78, F483*.

Levshin, A. L., M. H. Ritzwoller, and S. S. Smith (1996), "Group Velocity Variations Across Eurasia," in *Proceedings of the 18th Annual Seismic Research Symposium on Monitoring A Comprehensive Test Ban Treaty, 4-6 September, 1996*, Phillips Laboratory Report PL-TR-96-2153, July, pp. 70-79, ADA313692.

Mitchell, B. J., L. Cong and J. Xie, (1996), "Seismic Attenuation Studies in the Middle East and Southern Asia", St. Louis University Scientific Report No. 1, PL-TR-96-2154, ADA317387.

Mooney, W., G. Laske, and G. Masters (1998), "Crust 5.1: A Global Crustal Model at 5x5 Degrees," *Journal of Geophysical Research*, v. 103, no. B1, pp. 727-747.

Ritzwoller, M. H., A. L. Levshin, L. I. Ratnikova, and D. M. Tremblay (1996), "High Resolution Group Velocity Variations Across Central Asia," in *Proceedings of the 18th Annual Seismic Research Symposium On Monitoring A Comprehensive Test Ban Treaty, 4-6 September, 1996*, Phillips Laboratory Report PL-TR-96-2153, July, pp. 98-107, ADA313692.

Ritzwoller, M.H., O.Y Vdovin, and A.L. Levshin (1999), "Surface wave dispersion across Antarctica: A first look", *Antarctic J. U.S.*, in press.

Stevens, J. L. (1986), "Estimation of Scalar Moments From Explosion-Generated Surface Waves," *Bull. Seism. Soc. Am.*, v. 76, pp. 123-151.

Stevens, J. L., and D. A. Adams (1999), Improved surface wave detection and measurement using phase-matched filtering and improved regionalized models, 1999., *proceedings of the 21st Annual Seismic Research Symposium in Las Vegas, NV,* 274-282.

Stevens, J. L. and K. L. McLaughlin (1996), "Regionalized Maximum Likelihood Surface Wave Analysis," Maxwell Technologies Technical Report submitted to Phillips Laboratory, PL-TR-96-2273, SSS-DTR-96-15562, September, ADA321813.

Stevens, J. L., and K. L. McLaughlin (1988), "Analysis of surface waves from the Novaya Zemlya, Mururoa, and Amchitka test sites, and maximum likelihood estimation of scalar moments from earthquakes and explosions," S-CUBED technical report submitted to Air Force Technical Applications Center, SSS-TR-89-9953, September.

Stevens, J. L. and K. L. McLaughlin (2000), "Optimization of surface wave identification and measurement," *Pure and Applied Geophysics*, in press.

Vasco, D. W., L.R. Johnson, and O. Marques (1999), Global Earth structure: inference and assessment, *Geophys. J. Int.,* 137.

Vdovin, O. Y., J. A. Rial, M. H. Ritzwoller, and A. L. Levshin (1999), "Group-velocity tomography of South America and the surrounding oceans", *Geophys. J. Int.*, 136, 324-330.